STRUCTURAL CHEMISTRY

ISSN 2053-2296

Synthesis, structure and magnetocaloric properties of a new two-dimensional gadolinium(III) coordination polymer based on azobenzene-2,2′,3,3′-tetracarboxylic acid

Wen-Wen Wei,[a] Li-Ping Lu,[a]* Si-Si Feng,[a] Miao-Li Zhu[a] and Ulli Englert[a,b]*

[a]Institute of Molecular Science, Key Laboratory of Chemical Biology and Molecular Engineering of the Education Ministry, Shanxi University, 92 Wucheng Road, Taiyuan, Shanxi 030006, People's Republic of China, and [b]Institute of Inorganic Chemistry, RWTH Aachen University, Landoltweg. 1, Aachen 52074, Germany. *Correspondence e-mail: luliping@sxu.edu.cn, ullrich.englert@ac.rwth-aachen.de

Received 28 June 2021
Accepted 24 August 2021

Edited by E. Y. Cheung, Moderna Inc., USA

Keywords: azobenzenetetracarboxylic acid; Gd^{3+} coordination polymer; bridging carboxylate; antiferromagnetism; magnetocaloric effect; magnetic refrigeration; crystal structure.

CCDC reference: 2105211

Supporting information: this article has supporting information at journals.iucr.org/c

A new Gd^{3+} coordination polymer (CP), namely, poly[diaqua[μ_4-1′-carboxy-3,3′-(diazene-1,2-diyl)dibenzene-1,2,2′-tricarboxylato]gadolinium(III)], [Gd($C_{16}H_7N_2O_8$)(H_2O)$_2$]$_n$, (I), has been synthesized hydrothermally from $Gd(NO_3)_3\cdot 6H_2O$ and azobenzene-2,2′,3,3′-tetracarboxylic acid (H_4abtc). The target solid has been characterized by single-crystal and powder X-ray diffraction, elemental analysis, IR spectroscopy and susceptibility measurements. CP (I) crystallizes in the monoclinic space group $C2/c$. The structure features a 4-connected topology in which Gd^{3+} ions are connected by carboxylate groups into a linear chain along the monoclinic symmetry direction. Adjacent one-dimensional aggregates are bridged by $Habtc^{3-}$ ligands to form a two-dimensional CP in the $(10\bar{1})$ plane. A very short hydrogen bond [O$\cdots$O = 2.4393 (4) Å] links neighbouring layers into a three-dimensional network. A magnetic study revealed antiferromagnetic Gd$\cdots$Gd coupling within the chain direction. CP (I) displays a significant magnetocaloric effect (MCE), with a maximum $-\Delta S_m$ of 27.26 J kg^{-1} K^{-1} for ΔH = 7 T at 3.0 K. As the MCE in (I) exceeds that of the commercial magnetic refrigerant GGG ($Gd_3Ga_5O_{12}$, $-\Delta S_m$ = 24 J kg^{-1} K^{-1}, ΔH = 30 kG), CP (I) can be regarded as a potential cryogenic material for low-temperature magnetic refrigeration.

1. Introduction

Coordination polymers (CPs), a class of compounds based on repetition of metal cations connected by coordinated linkers, have developed rapidly in the past 20 years (Chakraborty *et al.*, 2021) due to their interesting structures and variable applications in gas storage and separation (Roztocki *et al.*, 2020), catalysis (Kang *et al.*, 2019), sensing (Lustig *et al.*, 2017) and magnetic materials (Yang *et al.*, 2019*a*). In particular, due to the unique 4*f* electron configuration of Ln^{3+} ions, lanthanide coordination polymers (Ln-CPs) usually exhibit a high coordination number, flexible coordination geometry and strong spin-orbit coupling (Sorace *et al.*, 2011; Liu *et al.*, 2016). These properties suggest their application in luminescence sensing (Ye *et al.*, 2017), molecular magnetism (Liu *et al.*, 2019), magnetic resonance imaging (Debroye & Parac-Vogt, 2014) and related fields (Kumar *et al.*, 2019).

Magnetic refrigeration represents a focus area in the field of magnetism. This approach is based on the magnetocaloric effect (MCE) (Yang *et al.*, 2015; Wu *et al.*, 2021) and is considered a highly efficient and energy-saving, hence environmentally friendly, technology. Key factors for success comprise a high-spin ground state *S*, negligible magnetic

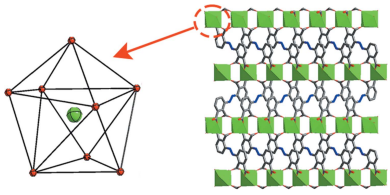

anisotropy and low-lying excited spin states (Evangelisti *et al.*, 2006; Liu *et al.*, 2014*a*). The basic principle of magnetic refrigeration is realized through repeated cycles of isothermal magnetization and adiabatic demagnetization through the MCE displayed by the magnetic materials (Han *et al.*, 2018). Magnetic refrigeration has potential for the generation of ultra-low temperatures. The magnitude of the MCE is usually measured by magnetic entropy change ($-\Delta S_m$) and adiabatic temperature change (ΔT_{ad}) under certain conditions (Franco *et al.*, 2018). A large ΔS_m under a relatively low magnetic field is mandatory for an attractive cryogenic magnetorefrigerant (Liu *et al.*, 2017). The $-\Delta S_m$ value of the well-known commercial low-temperature magnetic refrigeration material GGG ($Gd_3Ga_5O_{12}$) is 24 J kg^{-1} K^{-1} (ΔH = 30 kG) (Daudin *et al.*, 1982).

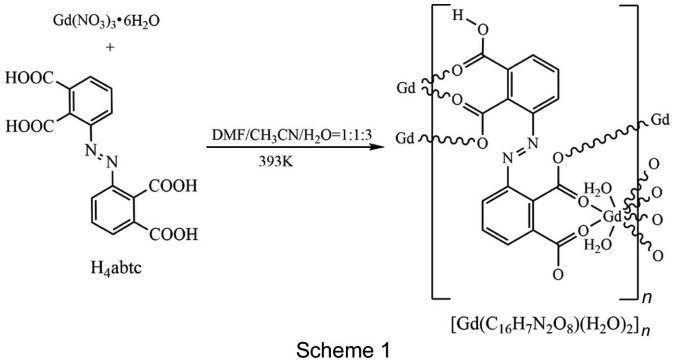

Scheme 1

The Gd^{3+} ion meets the requirements of a high-spin ground state *S* (*S* = 7/2), of low-lying excited spin states and magnetic isotropy (Niu *et al.*, 2019). The magnetic coupling between Gd^{3+} centres is relatively weak, which allows the system to achieve a large MCE (Zhang *et al.*, 2021). Therefore, the Gd^{3+} ion represents an ideal choice for the construction of molecular-based low-temperature magnetic refrigeration materials (Wang *et al.*, 2019). At present, molecular materials of cryogenic magnetic refrigeration mainly include Gd-based clusters and Gd-based CPs. However, the exploration of MCE for one-dimensional (1D) linear Gd^{3+} CPs has only rarely been documented (Liu *et al.*, 2014*b*).

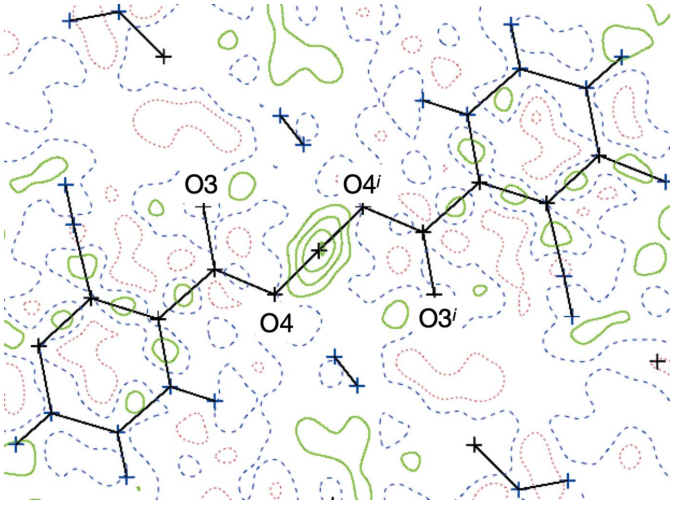

Figure 1
Difference Fourier map (*PLATON*; Spek, 2020) for (I) before inclusion of H4*A* into the structure model. Contour lines are drawn at an electron density of 0.1 e Å^{-3}. [Symmetry code: (i) $-x$, $-y+1$, $-z+1$.]

Table 1
Experimental details.

Crystal data	
Chemical formula	$[Gd(C_{16}H_7N_2O_8)(H_2O)_2]$
M_r	548.52
Crystal system, space group	Monoclinic, *C*2/*c*
Temperature (K)	298
a, *b*, *c* (Å)	25.725 (4), 5.0236 (9), 17.274 (3)
β (°)	127.393 (4)
V (Å^3)	1773.6 (5)
Z	4
Radiation type	Mo $K\alpha$
μ (mm^{-1})	3.80
Crystal size (mm)	0.20 × 0.15 × 0.15
Data collection	
Diffractometer	Bruker APEXII CCD
Absorption correction	Multi-scan (*SADABS*; Krause *et al.*, 2015)
T_{min}, T_{max}	0.600, 0.747
No. of measured, independent and observed [$I > 2\sigma(I)$] reflections	6278, 1568, 1508
R_{int}	0.024
(sin $\theta/\lambda)_{max}$ (Å^{-1})	0.598
Refinement	
$R[F^2 > 2\sigma(F^2)]$, $wR(F^2)$, *S*	0.013, 0.034, 1.11
No. of reflections	1568
No. of parameters	133
H-atom treatment	H atoms treated by a mixture of independent and constrained refinement
$\Delta\rho_{max}$, $\Delta\rho_{min}$ (e Å^{-3})	0.29, −0.33

Computer programs: *APEX2* (Bruker, 2009), *SAINT* (Bruker, 2009), *SHELXS97* (Sheldrick, 2008), *SHELXL2014* (Sheldrick, 2015) and *SHELXTL* (Bruker, 2009).

In view of the above-mentioned promising properties, we report the new two-dimensional (2D) Gd^{3+} complex, $[Gd(Habtc)(H_2O)_2]_n$, (I), for which we selected azobenzene-2,2′,3,3′-tetracarboxylic acid (H_4abtc) as the ligand. The four carboxylic acid groups of this rigid H_4abtc linker may be partially or completely deprotonated and thus show flexible and diverse coordination patterns. In one of these coordination modes, the O atoms of a carboxylate group can bridge Gd^{3+} ions and thus ensure magnetic exchange and transfer between adjacent Gd^{3+} ions, at the same time maintaining an overall rigid product (Zhang *et al.*, 2015*c*). In this article, we communicate the synthesis, structure and magnetic properties of (I).

2. Experimental

All reagents and solvents used were commercially available and were used without further purification. H_4abtc was purchased from Jinan Trading Company (China). FT–IR spectra were obtained with a Bruker TENSOR27 spectrometer on KBr disks in the 4000–400 cm^{-1} region. Elemental analyses (EAs) were performed using a PerkinElmer 240 elemental analyzer. Powder X-ray diffraction (PXRD) data were collected on a Bruker D8 Advance X-ray diffractometer (Cu $K\alpha$, λ = 1.5418 Å) at a rate of 10° min^{-1} in the 2θ range

5–50°. Based on the results of the single-crystal X-ray diffraction experiment, the simulated pattern was obtained with *Mercury* (Macrae *et al.*, 2020) assuming Cu $K\alpha_1$ radiation (λ = 1.54056 Å). The thermogravimetric analysis was performed on a Dupont thermal analyzer between room temperature and 1045 K under an N_2 flow with a heating rate of 10 K min^{-1}. Magnetic susceptibility was measured from a microcrystalline sample using a SQUID magnetometer (Quantum Design MPMS) in the range 2–300 K with a direct-current field of 1000 Oe. Isothermal field-dependent magnetization $M(H)$ was measured in the range 0–7 T from 2 to 10 K.

2.1. Synthesis and crystallization

The reaction route to (I) is shown in Scheme 1. $Gd(NO_3)_3{\cdot}6H_2O$ (67.7 mg, 0.15 mmol) and H_4abtc (35.8 mg, 0.1 mmol) were dissolved in a mixture of *N*,*N*-dimethylformamide (DMF, 2 ml), acetonitrile (CH_3CN, 2 ml) and distilled water (H_2O, 6 ml). The solution was sealed in a stainless steel container and heated under autogenous pressure at 393 K for 72 h. After this period, heating was suspended and the container was allowed to cool to room temperature. Yellow block-shaped crystals of the product were obtained by filtration, washed with water and dried in the air (yield 67%). Analysis calculated (%) for $C_{16}H_{11}GdN_2O_{10}$: C 35.01, H 2.01, N 5.10; found: C 35.05, H 2.02, N 5.13.

2.2. Refinement

Crystal data, data collection and structure refinement details are summarized in Table 1. Carbon-bound H atoms were placed in calculated positions and refined using a riding model, with aromatic C—H = 0.93 Å and $U_{iso}(H) = 1.2U_{eq}(C)$. The water H-atom positions were fixed as found (O—H distances are approximately 0.82 Å), with $U_{iso}(H) = 1.5U_{eq}(O)$. A difference Fourier map (Fig. 1) suggested Wyckoff position 4*b* for atom H4*A* in the short O···O contact, albeit as a very broad residual electron-density maximum. Our structure model with H4 in this special position therefore assumes a short symmetric hydrogen bond. In the absence of high-resolution or neutron data, we can neither disprove nor support a split-atom alternative and an asymmetric hydrogen bond. Şerb *et al.* (2011) have compiled structures featuring very short O···O bonds. The reflection conditions for the correct space group *C*2/*c* are also compatible with the subgroup *Cc*; tentative refinements in this noncentrosymmetric subgroup resulted in numerous high correlations and anticorrelations for positional and displacement parameters: 26 elements of the final inverted refinement matrix showed correlation coefficients with a modulus >0.9 and more than 100 with a modulus >0.8. These high correlations resulted in an unrealistically broad range of C—C bonds, and no convergence for physically meaningful displacement parameters could be achieved.

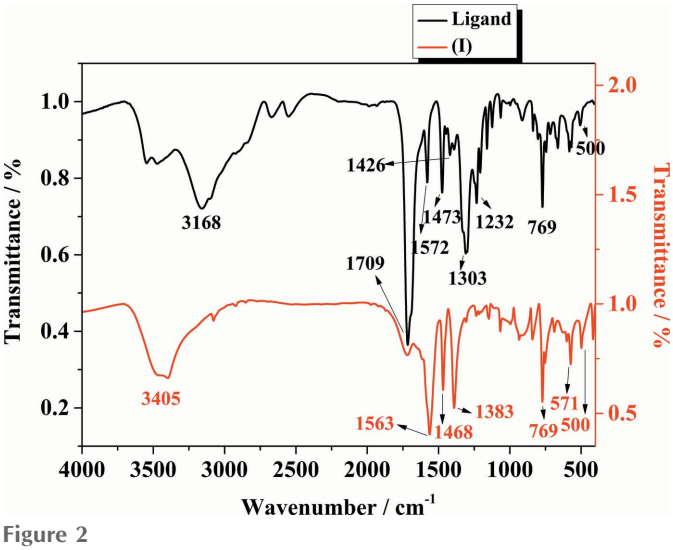

Figure 2
IR spectra of the ligand and (I).

3. Results and discussion

3.1. IR spectroscopy

The IR spectra of the ligand and (I) in the range 4000–400 cm^{-1} are presented in Fig. 2. The broad band at 3405 cm^{-1} indicates O—H stretching of the hydroxy groups and the coordinated water molecules in (I) (Yang *et al.*, 2019*b*). The characteristic absorption peaks of the asymmetric and symmetric stretching vibrations of the carboxylate groups appear at 1383 and 1563 cm^{-1} for (I) (Du *et al.*, 2016; Li *et al.*, 2012; Zhang *et al.*, 2015*a*). They are clearly shifted to lower wavenumbers in comparison with free H_4abtc (1426 and 1572 cm^{-1}), suggesting that the carboxylate groups in the complex are coordinated to the Gd^{3+} ions (An *et al.*, 2018). The absorption observed at 1468 cm^{-1} is caused by the N═N stretching vibration of the ligand (Goel & Kumar, 2018). The structural features of the complex deduced from IR spectra match the results of the single-crystal X-ray analysis. IR (KBr, ν, cm^{-1}, *s* = strong, *m* = medium and *w* = weak): 3405 (*m*), 1709 (*w*), 1563 (*s*), 1468 (*s*), 1383 (*s*), 1298 (*w*), 1147 (*w*), 1072 (*m*), 934 (*w*), 840 (*m*), 769 (*s*), 684 (*w*), 571 (*s*), 500 (*s*).

3.2. Structure description

Coordination polymer (I) crystallizes in the monoclinic space group *C*2/*c*, adopting a 2D framework based on coordination and covalent bonds; we originally expected a three-dimensional (3D) solid from the reaction between $Gd(NO_3)_3{\cdot}6H_2O$ and H_4abtc. The asymmetric unit of (I) contains a Gd^{3+} ion situated on a twofold axis (Wyckoff position 4*e*), one half of the $Habtc^{3-}$ ligand and a coordinated H_2O molecule. As shown in Fig. 3, each Gd^{3+} ion is eight-coordinated by O atoms in a $\{GdO_8\}$ environment, in which six O atoms [O1, O2, O3, $O1^i$, $O2^i$ and $O3^i$; symmetry code: (i) $-x, -y+1, -z+1$] are derived from the carboxylate groups of four $Habtc^{3-}$ moieties and two O atoms (O5 and $O5^i$) represent aqua ligands. The Gd—O distances are in the range 2.3449 (15)–2.4503 (16) Å and the O—Gd—O angles vary from 68.66 (5) to 149.37 (5)° (Table 2), consistent with values observed in related compounds (Nakamura *et al.*, 2021). The coordination polyhedron about the Gd^{3+} ion displays a

Table 2
Selected geometric parameters (Å, °).

Gd1—O1	2.3449 (15)	Gd1—O3	2.4446 (15)
Gd1—O2	2.3722 (15)	Gd1—O5	2.4502 (16)
O1—Gd1—O1^{i}	88.98 (8)	O3—Gd1—O3^{i}	139.00 (8)
O1—Gd1—O2	92.22 (6)	O1—Gd1—O5^{i}	140.25 (5)
O1—Gd1—O2^{i}	149.36 (5)	O1—Gd1—O5	80.69 (6)
O2—Gd1—O2^{i}	101.87 (8)	O2—Gd1—O5^{i}	78.93 (6)
O1—Gd1—O3	71.73 (5)	O2—Gd1—O5	69.85 (6)
O1—Gd1—O3^{i}	79.27 (5)	O3—Gd1—O5^{i}	68.66 (5)
O2—Gd1—O3	72.12 (5)	O3—Gd1—O5	131.45 (5)
O2—Gd1—O3^{i}	138.46 (5)	O5—Gd1—O5^{i}	129.63 (9)

Symmetry code: (i) $-x, y, -z+\frac{1}{2}$.

dicapped trigonal prismatic geometry, in which each Habtc^{3-} links four Gd^{3+} ions in a μ_4-η^1:η^1:η^1:η^0:η^1:η^1:η^1:η^0 coordination mode and all Gd^{3+} ions are connected *via* four bridging Habtc^{3-} ligands. Adjacent Gd^{3+} atoms are linked by the carboxylate groups of Habtc^{3-}, forming a linear Gd chain along [010]; the Gd···Gd separation corresponds to the lattice parameter *b* of 5.0236 (9) Å [Fig. 4(*a*)]. The 1D Gd chains are bridged by the central azo group of the Habtc^{3-} ligands to form a layer structure [Fig. 4(*b*)]. Two Habtc^{3-} ligands share the proton H4 which is located on a centre of inversion [see *Refinement* (§2.2) and Fig. 1] and plays the decisive role in linking adjacent coordination layers to a 3D framework [Fig. 4(*c*)]. In addition to this very short and symmetric hydrogen bond, the aqua ligand O5 acts as a hydrogen-bond donor towards carboxylate O atoms of a neighbouring layer. Detailed information of the intermolecular hydrogen bonds is summarized in Table 3. In order to obtain better insight into the nature of the intricate structure of CP (I), the network was simplified and its topology was analyzed with the help of the program *TOPOS* (Blatov & Shevchenko, 2006). As shown in Fig. 4(*d*), each Habtc^{3-} ligand can be perceived a four-

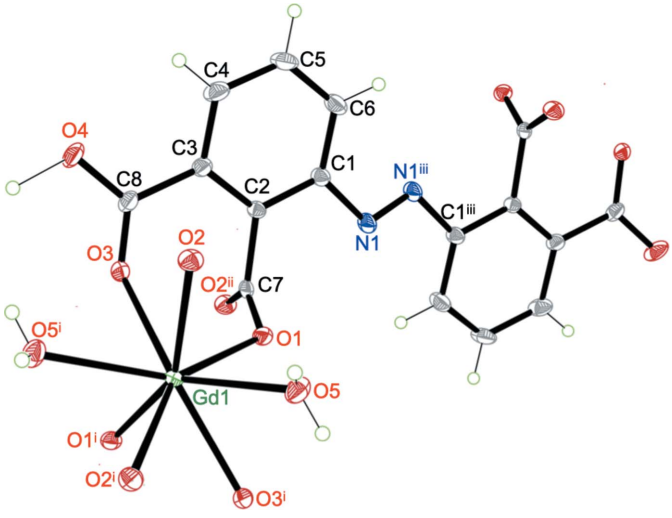

Figure 3
Expanded asymmetric unit and coordination environment of the Gd^{3+} ion in (I). Displacement ellipsoids are drawn at 30% probability and H atoms are represented as spheres of arbitrary radius. [Symmetry codes: (i) $-x, y, -z+\frac{1}{2}$; (ii) $x, y+1, z$; (iii) $-x+\frac{1}{2}, -y+\frac{5}{2}, -z+1$.]

Table 3
Hydrogen-bond geometry (Å, °).

D—H···*A*	*D*—H	H···*A*	*D*···*A*	*D*—H···*A*
O4—H4*A*···O3^{ii}	1.22	2.42	3.130 (2)	114
O4—H4*A*···O4^{ii}	1.22	1.22	2.439 (4)	180
O5—H5*A*···O1^{iii}	0.82	2.03	2.756 (2)	147
O5—H5*B*···O4^{iv}	0.82	2.01	2.821 (3)	173

Symmetry codes: (ii) $-x, -y+1, -z+1$; (iii) $x, y-1, z$; (iv) $x, -y+1, z-\frac{1}{2}$.

connected node towards Gd^{3+} ions and, *vice versa*, each Gd^{3+} ion is coordinated by four Habtc^{3-} ligands. The overall network can thus be described as a 4-connected net with the point symbol $(4^4\cdot6^2)$.

3.3. Powder X-ray diffraction (PXRD) and thermal stability

To verify the phase purity of the compound, the as-synthesized samples were characterized by PXRD at room temperature. As shown in Fig. 5(*a*), the experimental PXRD pattern of (I) is in excellent agreement with the simulated one, demonstrating the phase purity of the bulk sample. Minor differences in line intensities can probably be attributed to preferred orientation of the powder sample. Thermal stability was investigated by a thermogravimetric analysis (TGA) under an N_2 atmosphere. Fig. 5(*b*) summarizes the weight loss for (I) between room temperature and 1045 K. In the temperature range 325–471 K, the TGA curve shows a weight loss of 6.88% which may be attributed to the elimination of two coordinated water molecules (calculated 6.56%). At higher temperatures, the framework of (I) gradually collapses.

3.4. Magnetic properties

Magnetic properties of (I) were studied in order to understand potential magnetic interactions. Variable-temperature magnetic susceptibility measurements of (I) were conducted in the range 2–300 K with an applied magnetic field of 1000 Oe. As shown in Fig. 6, the experimental $\chi_m T$ value for (I) amounts to 8.00 cm^3 mol^{-1} K at 300 K, close to the expected value of 7.88 cm^3 mol^{-1} K calculated for an isolated Gd^{3+} ion (S = 7/2, g = 2) (Xi *et al.*, 2020). As the temperature is decreased, the $\chi_m T$ value of (I) decreases slowly to 7.93 cm^3 mol^{-1} K around 10 K, and then increases gradually to 8.14 cm^3 mol^{-1} K at 2 K. The data in the whole temperature range 2–300 K fit well the Curie–Weiss law with C = 8.06 cm^3 K mol^{-1} and θ = −0.08 K. The negative θ value indicates the existence of weak antiferromagnetic interactions between the metal centres in the 1D chain of (I). To further quantitatively analyze the magnetic interactions, the molar susceptibility of (I) can be described by a Fisher expression for a classical spin chain which allows an evaluation of the magnetic coupling (J) between adjacent Gd^{3+} ions (Farger *et al.*, 2018). The best least-squares fit parameters are g = 2.01 and J = −0.02 cm^{-1}, with an agreement factor $R = 6.27 \times 10^{-5}$ in the range 35–300 K. The value for J further proves the existence of weak antiferromagnetic interactions between adjacent Gd^{3+} ions in (I).

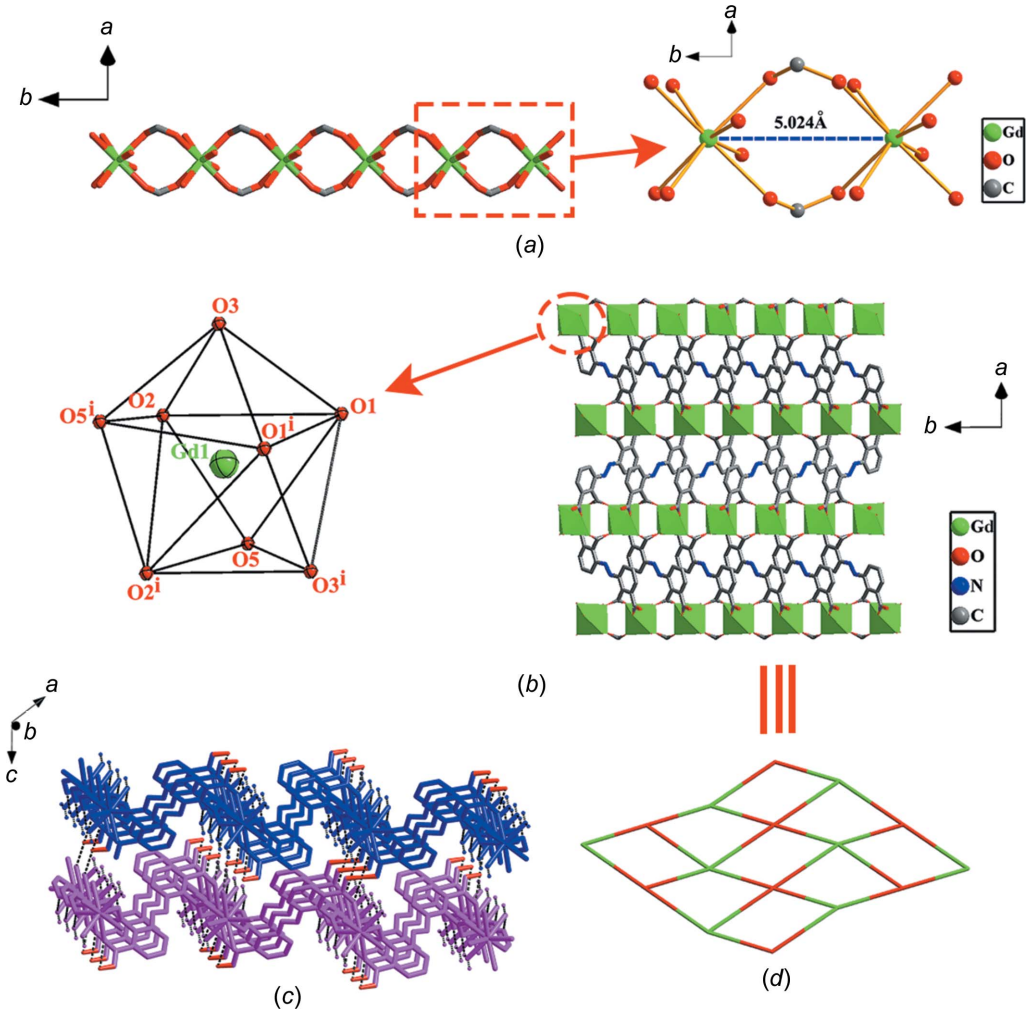

Figure 4
(*a*) Distances between adjacent Gd^{3+} ions in the 1D metal chain constructed by Gd^{3+} ions and the carboxylate groups of the $Habtc^{3-}$ ligands (H atoms have been omitted for clarity). (*b*) The 2D layer of (I). The inset is the local coordination geometry of the Gd^{3+} ion of (I). [Symmetry code: (i) $-x, y, -z+\frac{1}{2}$.] (*c*) The 3D framework formed by hydrogen bonds in (I) (different colours represent different layers and H4*A* atoms are shown in red). (*d*) The 2D topology of (I) with point symbol ($4^4 \cdot 6^2$).

The magnetization of (I) was measured in the interval between 0 and 7 T at temperatures between 2 and 10 K (Fig. 7*a*). The *M* values for (I) show a steady increase with increasing *H* and a saturation value of 7.14 Nβ at 7 T and 2 K, which is close to the expected value of $S \times g = 7/2 \times 2 = 7$ Nβ for an isolated Gd^{3+} ion ($S = 7/2$, $g = 2$). To evaluate the magne-

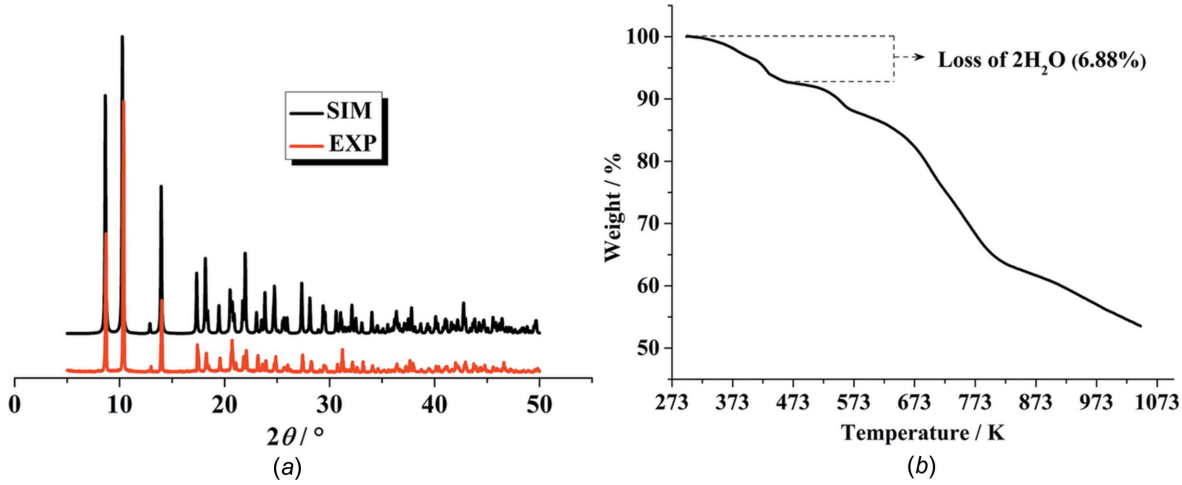

Figure 5
(*a*) Experimental and simulated PXRD patterns of (I) in the range 5–50°. (*b*) Thermogravimetric analysis for (I).

Table 4
Comparison of $-\Delta S_m$ for (I) and several previously reported 1D Gd^{3+} complexes.

OAc is acetate, pda is propanedionate, ox is oxalate, cit is citrate, piv is pivalate, MMA is methylmalonate, INA is isonicotinate, glu is glutamate, HPA is homophtalate, azdc is 4,4′-azobenzoate, phen is 1,10-phenanthroline, 2,5-TDA is thiophene-2,5-dicarboxylate, DMA is dimethylacetamide, DMF is dimethylformamide, N-BDC is 2-aminobenzene-1,4-dicarboxylate, mnba is *m*-nitrobenzoate, PAA is phenylacetate, HIN is isonicotinic acid and IN is isonicotinate.

Complex	Dimensionality	$-\Delta S_m^{max}$ (J kg^{-1} K^{-1})	Gd···Gd (Å)	M_W/N_{Gd}	Reference
$[Gd(OAc)_3(H_2O)_{0.5}]_n$	One-dimensional	50.4	4.0	343	Guo *et al.* (2012)
$[Gd(pda)(ox)_{0.5}]_n$	Three-dimensional	46.8	4.1–6.1	303	Liu *et al.* (2017)
$[Gd(pda)(ox)_{0.5}(H_2O)]_n$	Three-dimensional	46.1	4.3–6.3	321	Liu *et al.* (2017)
$[Gd(HCOO)(OAc)_2(H_2O)_2]_n$	One-dimensional	45.9	5.9	572	Lorusso *et al.* (2012)
$[Gd(OAc)_3(MeOH)]_n$	One-dimensional	45.0	4.1	366	Guo *et al.* (2012)
$[Gd(pda)(ox)_{0.5}(H_2O)_2]_n$	Two-dimensional	45.0	4.2–6.2	339	Liu *et al.* (2017)
$[Gd(cit)(H_2O)]_n$	Two-dimensional	43.6	4.5	363	Liu *et al.* (2014*b*)
$[Gd_2(piv)_5(\mu_3\text{-}OH)(H_2O)]_n$	One-dimensional	37.5	3.7	427	Liu *et al.* (2014*b*)
$[Gd(MMA)(INA)(H_2O)_2]_n$	Two-dimensional	36.0	4.7	431	Li *et al.* (2017*a*)
$\{[Gd_2(glu)_3(H_2O)_2]\cdot 4H_2O\}_n$	Three-dimensional	36.0	4.2	406	Zheng *et al.* (2017)
$\{[Gd(HPA)(NO_3)(H_2O)_2]\cdot H_2O\}_n$	One-dimensional	35.6	3.9	415	Li *et al.* (2017*b*)
$\{[Gd_2(HPA)_3(H_2O)_2]\cdot H_2O\}_n$	Two-dimensional	35.4	3.9	415	Li *et al.* (2017*b*)
$[Gd(azdc)(HCOO)]_n$	Three-dimensional	34.9	3.9	470	Zhang *et al.* (2015*b*)
$[Gd_2(MMA)_2(INA)_2(H_2O)_3]_n$	Two-dimensional	34.3	4.8	844	Li *et al.* (2017*a*)
$[Gd_2(SO_4)_3(phen)_2(H_2O)_2]_n$	One-dimensional	31.7	4.3	499	Zheng *et al.* (2017)
$[Gd_2(2,5\text{-}TDA)_3(DMA)_2]_n$	Three-dimensional	31.0	4.1	499	Kumar *et al.* (2020)
$\{[Gd_2(OH)_2L_2]\cdot DMF\cdot 4H_2O\}_n$	Three-dimensional	30.3	3.8–3.9	417	Peng *et al.* (2018)
$[Gd_2(N\text{-}BDC)_3(DMF)_4]_n$	Three-dimensional	29.0	10.5–12.1	366	Lorusso *et al.* (2012)
$[GdL_{1/2}(H_2O)_2]_n$	Two-dimensional	27.3	5.0	548	This work
$[Gd_2(mnba)_4(\mu\text{-}OH)_2(H_2O)]_n$	One-dimensional	27.1	3.8	515	Liu *et al.* (2014*b*)
$[Gd(PAA)_3(H_2O)]_n$	One-dimensional	26.7	4.0	580	Li *et al.* (2017*c*)
$\{Gd[IN][HIN][CH_2OCH_2O]\}_n$	One-dimensional	26.2	3.7	462	Li *et al.* (2020)
$\{[Gd_2(azdc)_3(DMA)_2]\cdot 2DMA\}_n$	Three-dimensional	22.3	4.6	734	Zhang *et al.* (2014)

tocaloric effect (MCE), the magnetic entropy change ($-\Delta S_m$) of (I) was calculated for a field between 0 and 7 T in the temperature range 2–10 K, and it can be obtained (Fig. 7*b*) by the Maxwell relation in the equation $\Delta S_m(T) = [M(T,H)/T]_H dH$. The resulting maximum value of $-\Delta S_m$ amounts to 27.26 J kg^{-1} K^{-1} for ΔH = 7 T at 3.0 K, which is smaller than the theoretical value of 31.52 J kg^{-1} K^{-1}, as calculated from the equation $-\Delta S_m = N_{Gd} R \ln(2s+1)/M_W$, with S = 7/2. In this equation, M_W is the formula mass of 548.52 g mol^{-1} and N_{Gd} is the number of Gd^{3+} ions present per mole of (I). The difference in $-\Delta S_m$ between the theoretical and experimental values may be attributed to the existence of antiferromagnetic interactions between Gd^{3+} ions. The experimental $-\Delta S_m$ value is also smaller than several previously prepared 1D linear-chain Gd^{3+} complexes (Table 4), which can be ascribed to the large M_W/N_{Gd} ratio arising from the large H_4abtc ligand and the antiferromagnetic interactions between the neighbouring Gd^{3+} ions in (I).

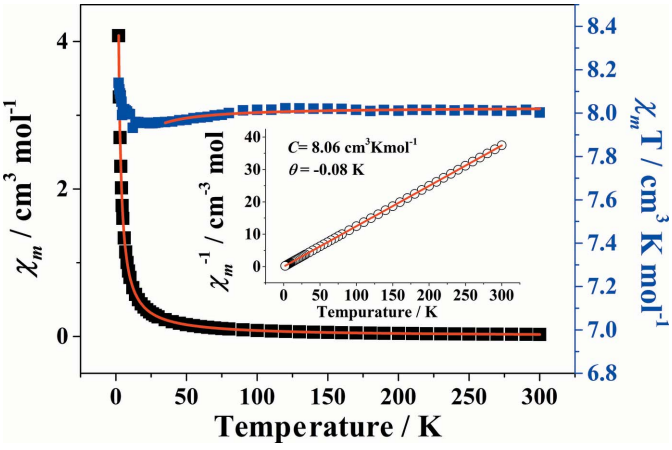

Figure 6
Plots of χ_m, $\chi_m T$ and χ_m^{-1} (inset) as functions of T for (I). Red solid lines represent best fits.

3.5. Conclusion

In summary, the novel coordination polymer (I) has been successfully constructed under hydrothermal conditions *via* the combination of Gd^{3+} ions and the H_4abtc linker. The underlying structural principles in (I) comprise a 1D $[Gd_2(COO)_4]_n$ chain and the linking of neighbouring chains *via* the organic ligand into a 2D structure with point symbol $(4^4\cdot 6^2)$. Further crosslinking into a 3D framework occurs *via* very short hydrogen bonds. The new CP offers potential for application; magnetic studies reveal that (I) displays intrachain antiferromagnetic Gd···Gd coupling and a cryogenic MCE with the maximum $-\Delta S_m$ of 27.26 J kg^{-1} K^{-1} for ΔH = 7 T at 3.0 K. This small $-\Delta S_m$ value can be ascribed to the high M_W/N_{Gd} ratio arising from the large H_4abtc ligand and the antiferromagnetic interactions between neighbouring Gd^{3+} ions in (I). The selection of low molecular-weight ligands that transfer weak coupling may be a promising approach for obtaining Gd^{3+} complexes as molecule-based magnetic refrigerants. Further studies on Gd^{3+} complexes for magnetic refrigeration are underway in our laboratory.

Acknowledgements

Open access funding enabled and organized by Projekt DEAL.

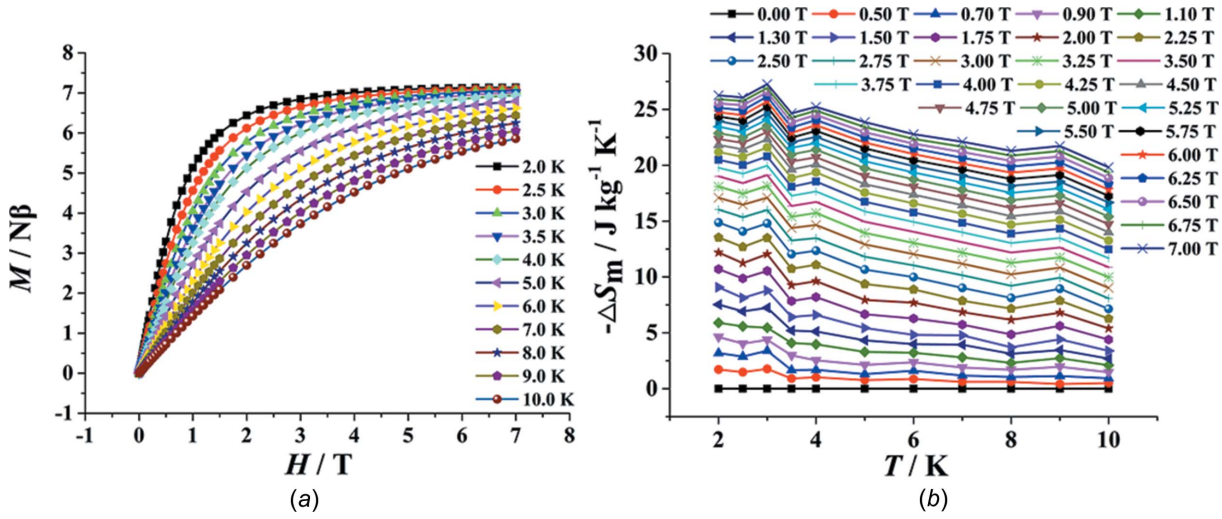

Figure 7
(*a*) *M versus H* plots from 2 to 10 K. (*b*) Calculated $-\Delta S_m$ from the magnetization data of (I) at various fields and temperatures.

Funding information

Funding for this research was provided by: National Natural Science Foundation of China (grant No. 21671124 to MLZ; grant No. 21571118 to LPL); One Hundred-Talent Program of Shanxi Province (award to UE); Shanxi University for academic research in Germany (award to WWW).

References

An, Y.-Y., Lu, L.-P. & Zhu, M.-L. (2018). *Acta Cryst.* C**74**, 418–423.

Blatov, V. A. & Shevchenko, A. P. (2006). *TOPOS*. Version 4.0. Samara State University, Samara, Russia.

Bruker (2009). *APEX2*, *SAINT* and *SHELXTL*. Bruker AXS Inc., Madison, Wisconsin, USA.

Chakraborty, G., Park, I. H., Medishetty, R. & Vittal, J. J. (2021). *Chem. Rev.* **121**, 3751–3891.

Daudin, B., Lagnier, R. & Salce, B. J. (1982). *J. Magn. Magn. Mater.* **27**, 315–322.

Debroye, E. & Parac-Vogt, T. N. (2014). *Chem. Soc. Rev.* **43**, 8178–8192.

Du, P. Y., Gu, W. & Liu, X. (2016). *CrystEngComm*, **18**, 5140–5148.

Evangelisti, M., Luis, F., de Jongh, L. J. & Affronte, M. (2006). *J. Mater. Chem.* **16**, 2534–2549.

Farger, P., Leuvrey, C., Gallart, M., Gilliot, P., Rogez, G., Rocha, J., Ananias, D., Rabu, P. & Delahaye, E. (2018). *Beilstein J. Nanotechnol.* **9**, 2775–2787.

Franco, V., Blázquez, J. S., Ipus, J. J., Law, J. Y., Moreno-Ramírez, L. M. & Conde, A. (2018). *Prog. Mater. Sci.* **93**, 112–232.

Goel, N. & Kumar, N. (2018). *RSC Adv.* **8**, 10746–10755.

Guo, F. S., Leng, J. D., Liu, J. L., Meng, Z. S. & Tong, M. L. (2012). *Inorg. Chem.* **51**, 405–413.

Han, Y., Han, S. D., Pan, J., Ma, Y. J. & Wang, G. M. (2018). *Mater. Chem. Front.* **2**, 2327–2332.

Kang, Y. S., Lu, Y., Chen, K., Zhao, Y., Wang, P. & Sun, W. Y. (2019). *Coord. Chem. Rev.* **378**, 262–280.

Krause, L., Herbst-Irmer, R. & Stalke, D. (2015). *J. Appl. Cryst.* **48**, 1907–1913.

Kumar, M., Li, L. Q., Zaręba, J. K., Tashi, L., Sahoo, S. C., Nyk, M., Liu, S. J. & Sheikh, H. N. (2020). *Cryst. Growth Des.* **20**, 6430–6452.

Kumar, M., Sheikh, H. N., Fraconetti, A., Zaręba, J. K., Sahoo, S. C. & Frontera, A. (2019). *New J. Chem.* **43**, 2179–2195.

Li, L. N., Wang, S. Y., Chen, T. L., Sun, Z. H., Luo, J. H. & Hong, M. C. (2012). *Cryst. Growth Des.* **12**, 4109–4115.

Li, N. F., Ji, J. Y., Jiang, W., Cao, J. P., Han, Y. M., Yuan, P. & Xu, Y. (2020). *Z. Anorg. Allg. Chem.* **646**, 463–468.

Li, Z. Y., Cao, Y. Q., Li, J. Y., Zhang, X. F., Zhai, B., Zhang, C., Zhang, F. L. & Cao, G. X. (2017*a*). *Cryst. Growth Des.* **17**, 6752–6761.

Li, Z. Y., Chen, Y., Dong, X. Y., Zhai, B., Zhang, X. F., Zhang, C., Zhang, F. L., Li, S. Z. & Cao, G. X. (2017*b*). *Cryst. Growth Des.* **17**, 3877–3884.

Li, Z. Y., Xu, Y. L., Zhang, X. F., Zhai, B., Zhang, F. L., Zhang, J. J., Zhang, C., Li, S. Z. & Cao, G. X. (2017*c*). *Dalton Trans.* **46**, 16485–16492.

Liu, C. M., Zhang, D. Q., Hao, X. & Zhu, D. B. (2019). *Cryst. Growth Des.* **19**, 4731–4737.

Liu, J. L., Chen, Y. C., Guo, F. S. & Tong, M. L. (2014*a*). *Coord. Chem. Rev.* **281**, 26–49.

Liu, K., Zhang, X. J., Meng, X. X., Shi, W., Cheng, P. & Powell, A. K. (2016). *Chem. Soc. Rev.* **45**, 2423–2439.

Liu, S. J., Cao, C., Yao, S. L., Zheng, T. F., Wang, Z. X., Liu, C., Liao, J. S., Chen, J. L., Li, Y. W. & Wen, H. R. (2017). *Dalton Trans.* **46**, 64–70.

Liu, S. J., Xie, C. C., Jia, J. M., Zhao, J. P., Han, S. D., Cui, Y., Li, Y. & Bu, X. H. (2014*b*). *Chem. Asian J.* **9**, 1116–1122.

Lorusso, G., Palacios, M., Nichol, G., Brechin, E., Roubeau, O. & Evangelisti, M. (2012). *Chem. Commun.* **48**, 7592–7594.

Lustig, W. P., Mukherjee, S., Rudd, N. D., Desai, A. V., Li, J. & Ghosh, S. K. (2017). *Chem. Soc. Rev.* **46**, 3242–3285.

Macrae, C. F., Sovago, I., Cottrell, S. J., Galek, P. T. A., McCabe, P., Pidcock, E., Platings, M., Shields, G. P., Stevens, J. S., Towler, M. & Wood, P. A. (2020). *J. Appl. Cryst.* **53**, 226–235.

Nakamura, T., Kanetomo, T. & Ishida, T. (2021). *Inorg. Chem.* **60**, 535–539.

Niu, H. J., Wang, L. H., Yang, G. E. & Wang, X. X. (2019). *Inorg. Chim. Acta*, **489**, 155–159.

Peng, D., Yin, L., Hu, P., Li, B., Ouyang, Z. W., Zhuang, G. L. & Wang, Z. X. (2018). *Inorg. Chem.* **57**, 2577–2583.

Roztocki, K., Szufla, M., Bon, V., Senkovska, I., Kaskel, S. & Matoga, D. (2020). *Inorg. Chem.* **59**, 10717–10726.

Şerb, M.-D., Wang, R., Meven, M. & Englert, U. (2011). *Acta Cryst.* B**67**, 552–559.

Sheldrick, G. M. (2008). *Acta Cryst.* A**64**, 112–122.

Sheldrick, G. M. (2015). *Acta Cryst.* C**71**, 3–8.

Sorace, L., Benelli, C. & Gatteschi, D. (2011). *Chem. Soc. Rev.* **40**, 3092–3104.

Spek, A. L. (2020). *Acta Cryst.* E**76**, 1–11.

Wang, Y. X., Xu, Q. T., Ren, P., Shi, W. & Cheng, P. (2019). *Dalton Trans.* **48**, 2228–2233.
Wu, S. M., Zhong, X. C., Dong, X. T., Liu, C. L., Huang, J. H., Huang, Y. L., Yu, H. Y., Liu, Z. W., Huang, Y. S. & Ramanujan, R. V. (2021). *J. Alloys Compd.* **873**, 159796.
Xi, L., Sun, J., Li, H. D., Han, J., Huang, X. H. & Li, L. C. (2020). *Cryst. Growth Des.* **20**, 3785–3794.
Yang, C. Q., Dong, R. H., Wang, M., Petkov, P. S., Zhang, Z. T., Wang, M. C., Han, P., Ballabio, M., Bräuninger, S. A., Liao, Z. Q., Zhang, J. C., Schwotzer, F., Zschech, E., Klauss, H. H., Cánovas, E., Kaskel, S., Bonn, M., Zhou, S. Q., Heine, T. & Feng, X. L. (2019*a*). *Nat. Chem.* **10**, 3260.
Yang, D.-D., Lu, L.-P. & Zhu, M.-L. (2019*b*). *Acta Cryst.* C**75**, 1580–1592.
Yang, Y., Zhang, Q. C., Pan, Y. Y., Long, L. & Zheng, L. S. (2015). *Chem. Commun.* **51**, 7317–7320.
Ye, J. W., Lin, J. M., Mo, Z. W., He, C. T., Zhou, H. L., Zhang, J. P. & Chen, X. M. (2017). *Inorg. Chem.* **56**, 4238–4243.
Zhang, H. T., Ma, L., Han, M. R., Feng, S. S. & Zhu, M. L. (2021). *Inorg. Nano-Met. Chem.* **51**, 761–765.
Zhang, J., Wang, C. C., Wang, P. & Gao, S. J. (2015*a*). *Transition Met. Chem.* **40**, 821–829.
Zhang, S. W., Duan, E., Han, Z. S., Li, L. L. & Cheng, P. (2015*b*). *Inorg. Chem.* **54**, 6498–6503.
Zhang, S. W., Ma, J. G., Zhang, X. P., Duan, E. Y. & Cheng, P. (2015*c*). *Inorg. Chem.* **54**, 586–595.
Zhang, S. W., Shi, W., Li, L. L., Duan, E. & Cheng, P. (2014). *Inorg. Chem.* **53**, 10340–10346.
Zheng, T. F., Yao, S. L., Cao, C., Liu, S. J., Hu, H. K., Zhang, T., Huang, H. P., Liao, J. S., Chen, J. L. & Wen, H. R. (2017). *New J. Chem.* **41**, 8598–8603.

supporting information

Acta Cryst. (2021). C**77**, 591-598 [https://doi.org/10.1107/S2053229621008871]

Synthesis, structure and magnetocaloric properties of a new two-dimensional gadolinium(III) coordination polymer based on azobenzene-2,2′,3,3′-tetracarboxylic acid

Wen-Wen Wei, Li-Ping Lu, Si-Si Feng, Miao-Li Zhu and Ulli Englert

Computing details

Data collection: *APEX2* (Bruker, 2009); cell refinement: *SAINT* (Bruker, 2009); data reduction: *SAINT* (Bruker, 2009); program(s) used to solve structure: *SHELXS97* (Sheldrick, 2008); program(s) used to refine structure: *SHELXL2014* (Sheldrick, 2015); molecular graphics: *SHELXTL* (Bruker, 2009); software used to prepare material for publication: *SHELXTL* (Bruker, 2009).

Poly[diaqua[μ_4-1′-carboxy-3,3′-(diazene-1,2-diyl)dibenzene-1,2,2′-tricarboxylato]gadolinium(III)

Crystal data

$[Gd(C_{16}H_7N_2O_8)(H_2O)_2]$
M_r = 548.52
Monoclinic, *C*2/*c*
a = 25.725 (4) Å
b = 5.0236 (9) Å
c = 17.274 (3) Å
β = 127.393 (4)°
V = 1773.6 (5) Å^3
Z = 4
F(000) = 1060
D_x = 2.054 Mg m^{-3}
Mo *Kα* radiation, *λ* = 0.71073 Å
Cell parameters from 5374 reflections
θ = 3.0–25.2°
μ = 3.80 mm^{-1}
T = 298 K
Block, yellow
0.20 × 0.15 × 0.15 mm

Data collection

Bruker APEXII CCD diffractometer
φ and *ω* scans
Absorption correction: multi-scan (*SADABS*; Krause *et al.*, 2015)
T_{min} = 0.600, T_{max} = 0.747
6278 measured reflections
1568 independent reflections
1508 reflections with $I > 2\sigma(I)$
R_{int} = 0.024
θ_{max} = 25.2°, θ_{min} = 3.0°
h = −30→29
k = −5→5
l = −20→20

Refinement

Refinement on F^2
Least-squares matrix: full
$R[F^2 > 2\sigma(F^2)]$ = 0.013
$wR(F^2)$ = 0.034
S = 1.11
1568 reflections
133 parameters
0 restraints
Primary atom site location: structure-invariant direct methods
Secondary atom site location: difference Fourier map
Hydrogen site location: mixed
H atoms treated by a mixture of independent and constrained refinement

$w = 1/[\sigma^2(F_o^2) + (0.0155P)^2 + 1.5784P]$
where $P = (F_o^2 + 2F_c^2)/3$
$(\Delta/\sigma)_{max} = 0.001$

$\Delta\rho_{max} = 0.29$ e Å^{-3}
$\Delta\rho_{min} = -0.33$ e Å^{-3}

Special details

Geometry. All esds (except the esd in the dihedral angle between two l.s. planes) are estimated using the full covariance matrix. The cell esds are taken into account individually in the estimation of esds in distances, angles and torsion angles; correlations between esds in cell parameters are only used when they are defined by crystal symmetry. An approximate (isotropic) treatment of cell esds is used for estimating esds involving l.s. planes.

Refinement. Single-crystal X-ray diffraction data for **(I)** were collected on a Bruker APEXII diffractometer equipped with 1 K CCD instrument, using a graphite monochromator with *Mo Kα* radiation (λ = 0.71073 Å) at room temperature. Absorption corrections were performed *via* the SADABS program (Bruker, 2001). All the structures were solved by means of direct methods with SHELXS-97 program (Sheldrick, 2008) and refined on F^2 with full-matrix least-squares techniques using the program SHELXL-2014 program (Sheldrick, 2015). All non-H atoms were refined anisotropically. H positions and isotropic displacement parameters constrained; H4a with refined Uiso on center of symmetry, hence coordinates fixed

Fractional atomic coordinates and isotropic or equivalent isotropic displacement parameters (Å²)

	x	*y*	*z*	U_{iso}*/U_{eq}
Gd1	0.000000	0.56130 (3)	0.250000	0.01598 (6)
O1	0.07997 (8)	0.8943 (3)	0.31251 (11)	0.0227 (3)
O2	0.07378 (8)	0.2637 (3)	0.37795 (11)	0.0262 (4)
O3	0.02231 (7)	0.7317 (3)	0.40008 (10)	0.0235 (3)
O4	0.05656 (10)	0.5732 (4)	0.54375 (14)	0.0499 (6)
H4A	0.000000 (1)	0.500000 (1)	0.500000 (1)	0.13 (3)*
O5	0.07156 (8)	0.3538 (4)	0.21824 (12)	0.0327 (4)
H5A	0.078437	0.195005	0.232767	0.049*
H5B	0.064136	0.369310	0.165148	0.049*
N1	0.22255 (9)	1.1967 (4)	0.47574 (13)	0.0253 (4)
C1	0.21412 (11)	1.0106 (5)	0.53013 (17)	0.0224 (5)
C2	0.14953 (11)	0.9340 (4)	0.48480 (16)	0.0187 (4)
C3	0.13547 (11)	0.7600 (5)	0.53305 (15)	0.0233 (5)
C4	0.18693 (13)	0.6585 (5)	0.62331 (17)	0.0339 (6)
H4	0.177983	0.544331	0.656255	0.041*
C5	0.25089 (12)	0.7240 (5)	0.66474 (18)	0.0360 (6)
H5	0.284663	0.647226	0.723624	0.043*
C6	0.26517 (12)	0.9030 (5)	0.61938 (18)	0.0316 (6)
H6	0.308258	0.950938	0.648062	0.038*
C7	0.09661 (10)	1.0408 (4)	0.38454 (16)	0.0186 (5)
C8	0.06676 (11)	0.6860 (5)	0.48759 (16)	0.0259 (5)

Atomic displacement parameters (Å²)

	U^{11}	U^{22}	U^{33}	U^{12}	U^{13}	U^{23}
Gd1	0.01432 (9)	0.01587 (9)	0.01428 (8)	0.000	0.00689 (7)	0.000
O1	0.0215 (8)	0.0262 (9)	0.0185 (8)	−0.0045 (6)	0.0112 (7)	−0.0014 (6)
O2	0.0275 (9)	0.0244 (9)	0.0251 (8)	0.0078 (7)	0.0151 (7)	0.0057 (7)
O3	0.0197 (8)	0.0306 (9)	0.0207 (8)	−0.0040 (6)	0.0125 (7)	−0.0025 (7)
O4	0.0400 (12)	0.0872 (17)	0.0256 (10)	−0.0310 (11)	0.0216 (9)	−0.0025 (10)

O5	0.0396 (10)	0.0347 (9)	0.0334 (9)	0.0130 (8)	0.0272 (9)	0.0112 (8)
N1	0.0181 (9)	0.0278 (11)	0.0261 (10)	−0.0058 (8)	0.0114 (8)	0.0019 (9)
C1	0.0185 (11)	0.0233 (11)	0.0210 (11)	−0.0035 (9)	0.0097 (10)	0.0010 (9)
C2	0.0176 (11)	0.0180 (11)	0.0174 (10)	−0.0015 (8)	0.0091 (9)	−0.0010 (9)
C3	0.0233 (12)	0.0259 (12)	0.0192 (11)	−0.0049 (9)	0.0122 (10)	0.0000 (9)
C4	0.0373 (14)	0.0352 (14)	0.0237 (12)	−0.0080 (12)	0.0157 (11)	0.0071 (11)
C5	0.0265 (13)	0.0404 (16)	0.0221 (12)	−0.0015 (11)	0.0048 (11)	0.0099 (11)
C6	0.0178 (12)	0.0374 (15)	0.0273 (13)	−0.0039 (10)	0.0074 (11)	0.0036 (11)
C7	0.0143 (10)	0.0218 (12)	0.0204 (11)	−0.0040 (9)	0.0108 (10)	0.0019 (9)
C8	0.0300 (13)	0.0303 (13)	0.0218 (12)	−0.0102 (11)	0.0180 (11)	−0.0041 (10)

Geometric parameters (Å, º)

Gd1—O1^{i}	2.3449 (15)	O5—H5B	0.8191
Gd1—O1	2.3449 (15)	N1—N1^{iii}	1.243 (4)
Gd1—O2	2.3722 (15)	N1—C1	1.432 (3)
Gd1—O2^{i}	2.3722 (15)	C1—C6	1.391 (3)
Gd1—O3	2.4446 (15)	C1—C2	1.393 (3)
Gd1—O3^{i}	2.4446 (15)	C2—C3	1.398 (3)
Gd1—O5^{i}	2.4502 (16)	C2—C7	1.509 (3)
Gd1—O5	2.4502 (16)	C3—C4	1.392 (3)
O1—C7	1.275 (3)	C3—C8	1.481 (3)
O2—C7^{ii}	1.237 (3)	C4—C5	1.377 (4)
O3—C8	1.243 (3)	C4—H4	0.9300
O4—C8	1.281 (3)	C5—C6	1.381 (4)
O4—H4A	1.2196	C5—H5	0.9300
O5—H5A	0.8224	C6—H6	0.9300
O1—Gd1—O1^{i}	88.98 (8)	C8—O3—Gd1	132.45 (15)
O1^{i}—Gd1—O2	149.37 (5)	C8—O4—H4A	112.33
O1—Gd1—O2	92.22 (6)	Gd1—O5—H5A	113.3
O1^{i}—Gd1—O2^{i}	92.22 (6)	Gd1—O5—H5B	120.9
O1—Gd1—O2^{i}	149.36 (5)	H5A—O5—H5B	107.1
O2—Gd1—O2^{i}	101.87 (8)	N1^{iii}—N1—C1	113.7 (2)
O1^{i}—Gd1—O3	79.27 (5)	C6—C1—C2	121.1 (2)
O1—Gd1—O3	71.73 (5)	C6—C1—N1	124.3 (2)
O1^{i}—Gd1—O3^{i}	71.73 (5)	C2—C1—N1	114.6 (2)
O1—Gd1—O3^{i}	79.27 (5)	C1—C2—C3	119.3 (2)
O2—Gd1—O3	72.12 (5)	C1—C2—C7	118.92 (19)
O2^{i}—Gd1—O3	138.46 (5)	C3—C2—C7	121.8 (2)
O2—Gd1—O3^{i}	138.46 (5)	C4—C3—C2	118.8 (2)
O2^{i}—Gd1—O3^{i}	72.11 (5)	C4—C3—C8	121.3 (2)
O3—Gd1—O3^{i}	139.00 (8)	C2—C3—C8	119.9 (2)
O1^{i}—Gd1—O5^{i}	80.69 (6)	C5—C4—C3	121.2 (2)
O1—Gd1—O5^{i}	140.25 (5)	C5—C4—H4	119.4
O1^{i}—Gd1—O5	140.25 (5)	C3—C4—H4	119.4
O1—Gd1—O5	80.69 (6)	C4—C5—C6	120.4 (2)
O2—Gd1—O5^{i}	78.93 (6)	C4—C5—H5	119.8

O2^{i}—Gd1—O5^{i}	69.86 (6)	C6—C5—H5	119.8
O2—Gd1—O5	69.85 (6)	C5—C6—C1	119.0 (2)
O2^{i}—Gd1—O5	78.93 (6)	C5—C6—H6	120.5
O3—Gd1—O5^{i}	68.66 (5)	C1—C6—H6	120.5
O3^{i}—Gd1—O5^{i}	131.45 (5)	O2^{iv}—C7—O1	125.0 (2)
O3—Gd1—O5	131.45 (5)	O2^{iv}—C7—C2	118.32 (19)
O3^{i}—Gd1—O5	68.66 (5)	O1—C7—C2	116.69 (18)
O5—Gd1—O5^{i}	129.63 (9)	O3—C8—O4	122.9 (2)
C7—O1—Gd1	122.79 (13)	O3—C8—C3	121.22 (19)
C7^{ii}—O2—Gd1	136.28 (14)	O4—C8—C3	115.9 (2)
N1^{iii}—N1—C1—C6	−16.0 (4)	C2—C1—C6—C5	−2.1 (4)
N1^{iii}—N1—C1—C2	166.3 (3)	N1—C1—C6—C5	−179.7 (2)
C6—C1—C2—C3	4.4 (3)	Gd1—O1—C7—O2^{iv}	−94.9 (2)
N1—C1—C2—C3	−177.8 (2)	Gd1—O1—C7—C2	86.9 (2)
C6—C1—C2—C7	−175.3 (2)	C1—C2—C7—O2^{iv}	−83.3 (3)
N1—C1—C2—C7	2.4 (3)	C3—C2—C7—O2^{iv}	97.0 (3)
C1—C2—C3—C4	−2.9 (3)	C1—C2—C7—O1	95.1 (2)
C7—C2—C3—C4	176.8 (2)	C3—C2—C7—O1	−84.7 (3)
C1—C2—C3—C8	177.4 (2)	Gd1—O3—C8—O4	−114.6 (2)
C7—C2—C3—C8	−2.9 (3)	Gd1—O3—C8—C3	65.3 (3)
C2—C3—C4—C5	−0.8 (4)	C4—C3—C8—O3	−165.5 (2)
C8—C3—C4—C5	178.9 (3)	C2—C3—C8—O3	14.2 (4)
C3—C4—C5—C6	3.1 (4)	C4—C3—C8—O4	14.4 (4)
C4—C5—C6—C1	−1.6 (4)	C2—C3—C8—O4	−165.9 (2)

Symmetry codes: (i) −*x*, *y*, −*z*+1/2; (ii) *x*, *y*−1, *z*; (iii) −*x*+1/2, −*y*+5/2, −*z*+1; (iv) *x*, *y*+1, *z*.

Hydrogen-bond geometry (Å, º)

D—H···*A*	*D*—H	H···*A*	*D*···*A*	*D*—H···*A*
O4—H4*A*···O3^{v}	1.22	2.42	3.130 (2)	114
O4—H4*A*···O4^{v}	1.22	1.22	2.439 (4)	180
O5—H5*A*···O1^{ii}	0.82	2.03	2.756 (2)	147
O5—H5*B*···O4^{vi}	0.82	2.01	2.821 (3)	173

Symmetry codes: (ii) *x*, *y*−1, *z*; (v) −*x*, −*y*+1, −*z*+1; (vi) *x*, −*y*+1, *z*−1/2.